J Mater Sci: Mater Med (2010) 21:1503–1510
DOI 10.1007/s10856-010-4009-5

Mechanical strength of extrusion freeformed calcium phosphate filaments

H. Y. Yang · X. P. Chi · S. Yang · J. R. G. Evans

Received: 27 November 2009 / Accepted: 25 January 2010 / Published online: 10 February 2010

Abstract Hydroxyapatite–tricalcium phosphate mixtures of various compositions were extruded by a solid freeforming process to form lattice structures to serve as hard tissue scaffolds. The unwelded filaments, sintered at temperatures from 1100 to 1300°C, had radii from 115 to 135 μm and were tested in three point flexural loading using a purpose-built fixture. Flexural strength ranged from 20 to 100 MPa depending on composition and sintering temperature. Weibull moduli up to 13 were obtained. Compositions with 50% or more tri-calcium phosphate did not develop strengths much above 40 MPa and the strength of most compositions fell when the sintering temperature exceeded 1250°C. Multiple layer lattice structures were created and tested in compression.

1 Introduction

A large and diverse range of calciferous minerals have been used to promote the repair and growth of bone following invasive surgery. They include hen's eggshell, ostrich eggshell, bovine cancellous bone, plaster of Paris and marine coral [1, 2]. In order to acquire greater compositional control of such bone substitute or scaffold materials, synthetic ceramic foams have been prepared using calcium phosphates of various phase composition [3–5]. Nevertheless, foams allow limited control over pore structure which is strongly influenced by nucleation, surface tension and elongational viscosity. There is something to be said for using the emergent solid freeforming/rapid prototyping processes [6, 7] to obtain structural control over porous materials. These are well known for reproducing the shape of a biomaterial from, for example, CT data but less well known for their ability to reproduce compositional [8, 9] and potentially microstructural design from a computer file. Various solid freeforming techniques have been used in this way including stereolithography [10], selective laser sintering [11], 3D printing [12] and extrusion freeforming [13].

Extrusion freeforming makes use of a ceramic paste comprising a polymer vehicle and a volatile solvent and produces solidification by solvent evaporation. The method is similar to fused deposition of ceramics (FDC) [14], multiphase jet solidification (MJS) [15] and Robocasting™ [16]. Instead of making use of melting and solidification, polymerization reactions or dilatant transitions to establish a change of state, it takes advantage of the evaporation of solvent to change a polymer solution to a gel. The solvent chosen is propan-2-ol, widely used as a disinfectant in hospitals. Lattice scaffolds are prepared in which each filament welds to the previous layer by growth of the contact area driven by surface energy decrease and resisted by viscosity. In this way, lattice scaffolds with hierarchical levels of porosity which could include a network of large channels intended to allow vascularisation and macroscopic outline shape are established in a computer file, downloaded directly to a building platform and subsequently sintered.

Calcium phosphate based materials, such as hydroxyapatite (HA) and tricalcium phosphate (TCP) are used in implants for orthopaedic and dental applications [17], for bone augmentation, plastic reconstruction, drug delivery

H. Y. Yang · X. P. Chi · S. Yang
Department of Materials, Queen Mary, University of London, Mile End Road, London E14 NS, UK

J. R. G. Evans (✉)
Department of Chemistry, University College London, 20 Gordon Street, London WC1H 0AJ, UK
e-mail: j.r.g.evans@ucl.ac.uk

systems [18], and bone tissue engineering [12] in the form of blocks, discs, granules or porous scaffolds. These minerals are selected for their osteogenicity not for their mechanical properties, which criterion, if given priority might well exclude them. The plane strain fracture toughness of HA is about 1 MPa $m^{1/2}$ [19, 20] and mechanical strength of material prepared by fully sintering HA powder is in the region of 120 MPa at best [19].

HA/TCP lattices have been successfully fabricated using extrusion freeforming [21] and to optimize the strength of these lattices using numerical methods, the mechanical properties of the filament are needed. To this end, HA and β-TCP, meeting ASTM F1185-03 and F1088-04a specifications for clinical applications were used in different ratios as starting materials for filament extrusion. Filament strength was measured in terms of phase composition and sintering temperature using a purpose built, small scale, 3 point loading test fixture.

2 Experimental details

The hydroxyapatite ($Ca_{10}(PO_4)_6(OH)_2$, Grade P221 S, Plasma Biotal Ltd. UK) and β-tricalcium phosphate ($Ca_3(PO_4)_2$, Grade P228 S, Plasma Biotal Ltd UK) powders were prepared by the manufacturer by calcining at 900°C and milling in water for 96 h. Poly(vinyl butyral) (PVB), grade BN18 (Wacker Chemicals, Germany) was used as the binder with additions of a grade of poly(ethylene glycol) (PEG) that is liquid at ambient temperature, (MWt = 600, VWR, UK).

In order to prepare pastes for extrusion, mixtures of 75 wt% PVB and 25 wt% PEG600 were dissolved in propan-2-ol (GPR, VWR, UK). Independently, powder mixtures having HA contents of 25, 50, 75 and 100 wt% (the remainder being TCP) were dispersed in propan-2-ol with an ultrasonic probe (IKA U200S, IKA Labortechnik Staufen, Germany) for 15 min. These were mixed to provide a ceramic/polymer mixture with 60 vol% ceramic powder based on the dry mass. These mixtures were placed on a roller table with zirconia media for 12 h. Partial drying was used to reach a solvent level suitable for extrusion with intermittent stirring and the final solvent content was measured by drying a sample to constant mass at 60°C.

The extrusion freeforming rig consists of a three axis table of which the *X* and *Y* axes are driven by linear motors to give high accelerations. The extruder barrel consists of a syringe (HGB81320 1 ml, Hamilton GB, Ltd, Carnforth, U.K.) driven by micro-stepper motors (50,000 steps/rev) supplied by ACP&D Ltd, Ashton-under-Lyne, UK, with a 64-1 reduction box driving 1 mm pitch ball screws (Automotion Ltd, Oldham, UK) over a three axis table (Parker Hannifin Automation, Dorset, UK). Extrusion dies of 80, 100, 150 and 300 μm diameter were purchased from Quick-OHM (Sapphire water-jet cutting nozzle, models 1708, 1710, 1715 and 1730, Germany). The table was driven by Labview™ software to form latticework patterns. Filaments of 100 mm length and 300 μm diameter were extruded and cut into 80 mm length for sintering and subsequent flexural strength testing. After drying, the extruded filaments were heated in 5 groups at 5°C/min to 1100, 1150, 1200, 1250 and 1300°C with a 5 h dwell before furnace cooling to room temperature.

The cross sections and surfaces of the filaments both sintered and unsintered were observed by scanning electron microscopy (SEM, Jeol 6300, Japan). The density and porosity of filaments were calculated by measuring the mass and diameter of the cross section of 80 mm long filaments, the diameters being measured from the SEM images, three samples were used for each test.

XRD analysis of the ceramic was recorded on a diffractometer (Model D5000, Siemens, Karlsruhe, Germany) using CuKα radiation. The step size was 0.02° 2θ with a count time of 2.5 s. Phases were identified using the International Centre for Diffraction Data powder diffraction files (No. 9-432 for HAP, No. 9-169 for β-TCP, and No. 9-348 for α-TCP). Peaks (2 1 0) for HA and (0 2 10) for β-TCP were used to calculate the ratios of intensities.

A miniature three point loading fixture (Fig. 1) was constructed to fit the microextrusion apparatus to convert it to a loading frame. It was designed to accommodate cylindrical samples of length 20 mm and diameters in the region 230–270 μm using ASTM C 1161-94 as a guide (the dimensions are well below its specified ranges). Thus, the diameter of the bearing cylinders was 0.41 mm being approximately 1.5 times the beam depth of the test specimen. Its maximum deflection, calculated for span L = 8 mm, sample dia. 0.27 mm at a sample failure stress of 150 MPa was 0.2% of the length of the pin. The load was measured using a strain gauge (FLA-2-11, Tokyo Sokki Kenkyujo Co. Ltd.) attached to a hardened steel cantilevered beam of thickness 100 μm. The strain gauge was connected to a bridge comprising wire-wound precision resistors and the output connected to a chart recorder, the voltage scale of which was calibrated from a high precision digital voltage supply (Model 230 Keithley Instruments). The deflection of the beam, as recorded by the output of the strain gauge bridge, was calibrated by applying the loading pin to a balance (TR104, Dover, USA) which was first calibrated with known weights from 2 mg to 1 g (and gave a maximum deviation of 0.1% at 100 mg). During flexural testing of filaments, the cross head speed was kept at 4 μm s^{-1}.

The compression testing of bulk sintered lattices was also conducted in an attempt to deduce the nominal

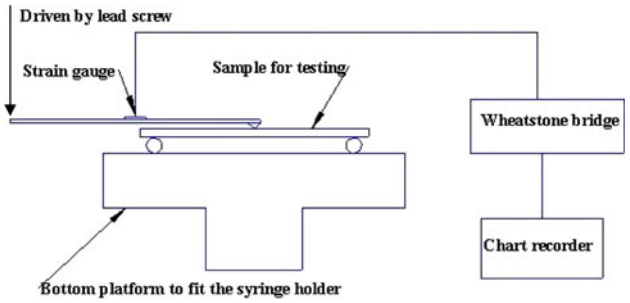

Fig. 1 Schematic diagram of the miniature three point flexural loading apparatus which was mounted on the press axis of the micro-extruder

flexural strength of the material from the Ashby equation and thus relate it to the flexural testing of individual filaments. Extruded HA lattices with filament diameters of 300 μm and inter-filament gaps of 200, 300 and 400 μm were sintered at 1250°C and those with a gap of 300 μm were sintered at 1150, 1250 and 1300 °C. The lattices were observed by optical microscopy (Model BX60, Olympus, Japan). The structural apparent density of each lattice was calculated from the filament diameters and spacings. Mechanical testing was conducted on a 5 kN Instron testing machine (4465, Instron Corp., USA) with a crosshead speed of 0.2 mm/min. Compression pads consisting of natural rubber were inserted between sample and platens to compensate for imperfect parallels. Compressive strength was derived from a load-deformation curve using the measured cross-sectional area and the steady crushing load.

3 Results and discussion

3.1 Compression testing

Figure 2 shows the construction of a compression test sample using a 300 μm diameter die and Fig. 3 shows examples of lattices made with different filament spacings. A set of lattices each with 20 layers was prepared for compression testing of whole lattices. The difference in filament spacing produces different levels of macroporosity which has a strong influence on compressive strength as shown in Fig. 4. With tall builds there is often a slight curvature of the upper layers caused by drying shrinkage which may affect compression testing (Fig. 4a). For this reason soft pads were installed between the platen and the sample. For a conventional ceramic foam, the early stage of compression involves an ascending load curve and it is only when steady collapse under a near-constant load is obtained that a compressive strength can be recorded [22].

This ideal behaviour was not always fully developed. An example of a compression loading trace is shown in Fig. 4b. The long upward sweep of load is partly due to compliance of the rubber pads used to overcome misalignment arising from slight curvature due to drying shrinkage. Tests were stopped at about 25% strain and the downward curve represents recovery of these inserts. The ratio of pore size to sample size is much greater than in a conventional ceramic foam test-piece and so the averaging of load during progressive collapse of layers as demonstrated by Gibson and Ashby for a conventional foam [22] led to much greater variability. Large error bars therefore attend the compression testing results.

Lattices made with 100HA and sintered at increasing temperatures from 1150°C to 1300°C (Fig. 4c) have compressive strengths that increase by a factor of approximately three which coincides with the increase in single filament tensile strength discussed below (Table 2). The compressive strength of a series of lattices sintered at 1250°C but with different macro-porosities are shown in Fig. 4d. These differ in the gap between filaments which was set at 0.2, 0.3 and 0.4 mm before sintering and gave structural (i.e. macro) porosities of 52.9, 60.7 and 66.3% after sintering, respectively. A doubling of the gap between filaments caused the compressive strength to fall by half. There is an expected decrease of compressive strength with porosity which, for a conventional foam, would fit the Gibson and Ashby equation:

$$\sigma_c = C\sigma_f \left(\frac{\rho}{\rho_{th}}\right)^{\frac{3}{2}} \quad (1)$$

in which c is a constant in the region 2–3, σ_f is the flexural strength of the struts, ρ is the apparent density and ρ_{th} is the theoretical density of the ceramic. The results are plotted in this way in Fig. 4d from which the value of $C\sigma_f$ is 45 MPa. As can be seen from Table 2, the flexural strength of 100HA sintered at 1250°C was 54 MPa which means for this structural geometry, C is in the region 0.8–0.9 rather than 2–3. It is unsurprising that this constant should differ because the scaffolds are structurally quite different from foams.

The failure mode of the lattices was therefore observed with a particular interest in seeing if weld failure could be detected. Figure 5 shows that, in general, filaments fracture adjacent to the welds so that the ends of remaining filaments are seen either directly above or just beyond the weld region. This implies that the welds act as loading supports and failure takes place adjacent to them. In a formal sense, the welds are loaded in uniform compression but structural misalignment means that bending and torsion are present.

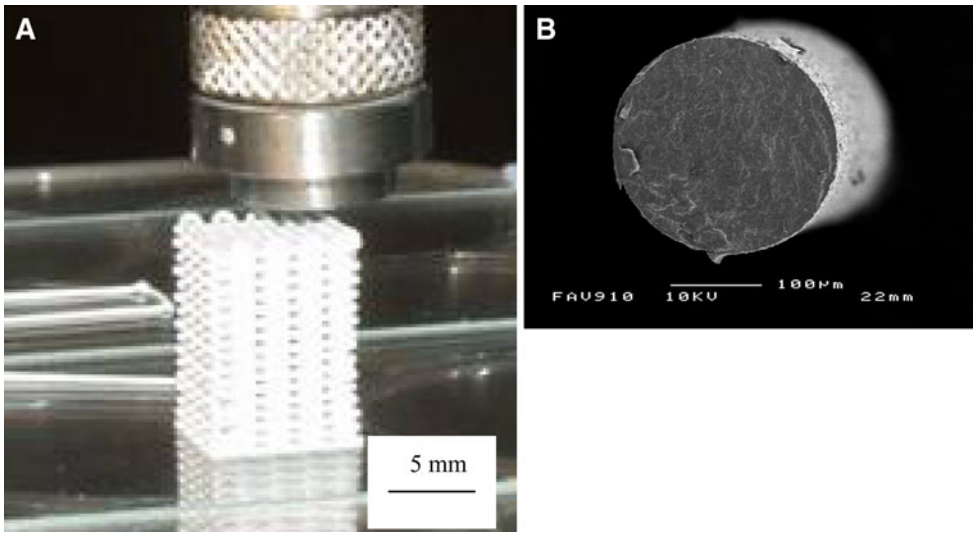

Fig. 2 **a** Photograph showing the construction of a compression test sample. **b** Fracture face of a filament sintered at 1300°C

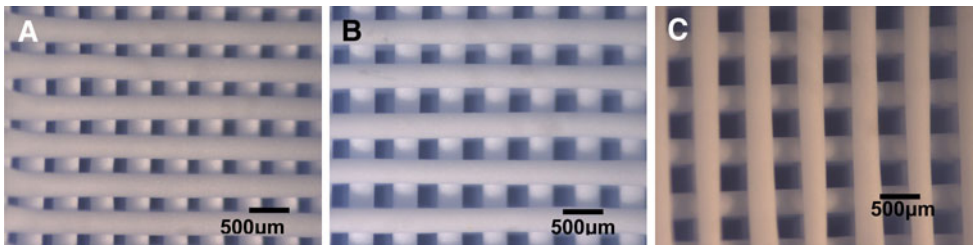

Fig. 3 Optical micrographs of the lattices with filament spacings: **a** 200 µm; **b** 300 µm and **c** 400 µm

3.2 Flexural testing of filaments

Using Rahaman's [23] designation of three sintering stages, all samples sintered at 1100°C are in the initial stage typified by relative density $\rho/\rho_{th} < 0.65$, with initial neck growth between particles and low mechanical strength. Conversely, when sintered at or above 1250°C, all samples are in the final stage, having $\rho/\rho_{th} > 0.9$, with disappearance of closed porosity and more extensive grain growth. The transformation of a small amount of β-TCP to α-TCP causes a slight decrease in theoretical density and is not taken into account in this calculation, so relative densities of filaments sintered at 1300°C are slightly underestimated in the calculation and this effect is more pronounced in the β-TCP-rich samples. When sintered at 1200°C and 1150°C, the relative densities for most samples in the intermediate stage are in the range of $\rho/\rho_{th} = 0.65$–0.9, showing progressive disappearance of open porosity.

The effect of sintering temperature is slightly different on each composition and gives rise to different porosity and filament diameters as shown in Table 1. The general trend up to 1200°C is that as the TCP content and sintering temperature increase, the shrinkage is greater and filament diameter is reduced.

The flexural strengths of individual filaments measured in three point loading using the specially constructed and calibrated fixture described above are shown in Table 2. If Tables 1 and 2 are compared, the effects of sintering temperature on strength, shrinkage and porosity are as expected up to 1250°C. The 25HA and 50HA materials initially have somewhat higher strength than the compositions with more HA but there is very little increase in strength as sintering progresses and these compositions barely manage to develop strength beyond 40 MPa. The 75HA and 100HA filaments demonstrate development of strength during sintering that makes them more interesting structurally. At 1250°C the 75HA samples show extensive sintering and this is reflected in the high flexural strength of 102 MPa. A sintering temperature of 1250°C has generally been found to be the maximum for HA. For example, a hydrothermally produced fine (100 nm) powder presented

Table 1 Filament diameters and porosities (in parenthesis) of filaments as a function of sintering temperature and composition

Sintered filament diameter/µm (porosity)					
Comp[n].	1100°C	1150°C	1200°C	1250°C	1300°C
100HA	272(0.36)	265(0.31)	255(0.23)	247(0.08)	240(0.04)
75HA	270(0.36)	264(0.32)	250(0.20)	236(0.04)	234(0.02)
50HA	267(0.37)	263(0.32)	245(0.12)	236(0.08)	236(0.06)
25HA	263(0.37)	250(0.27)	243(0.13)	236(0.10)	230(0.08)

* Diameters were measured by SEM images ($n = 3$) and the dimensional tolerances are typically ±5 µm

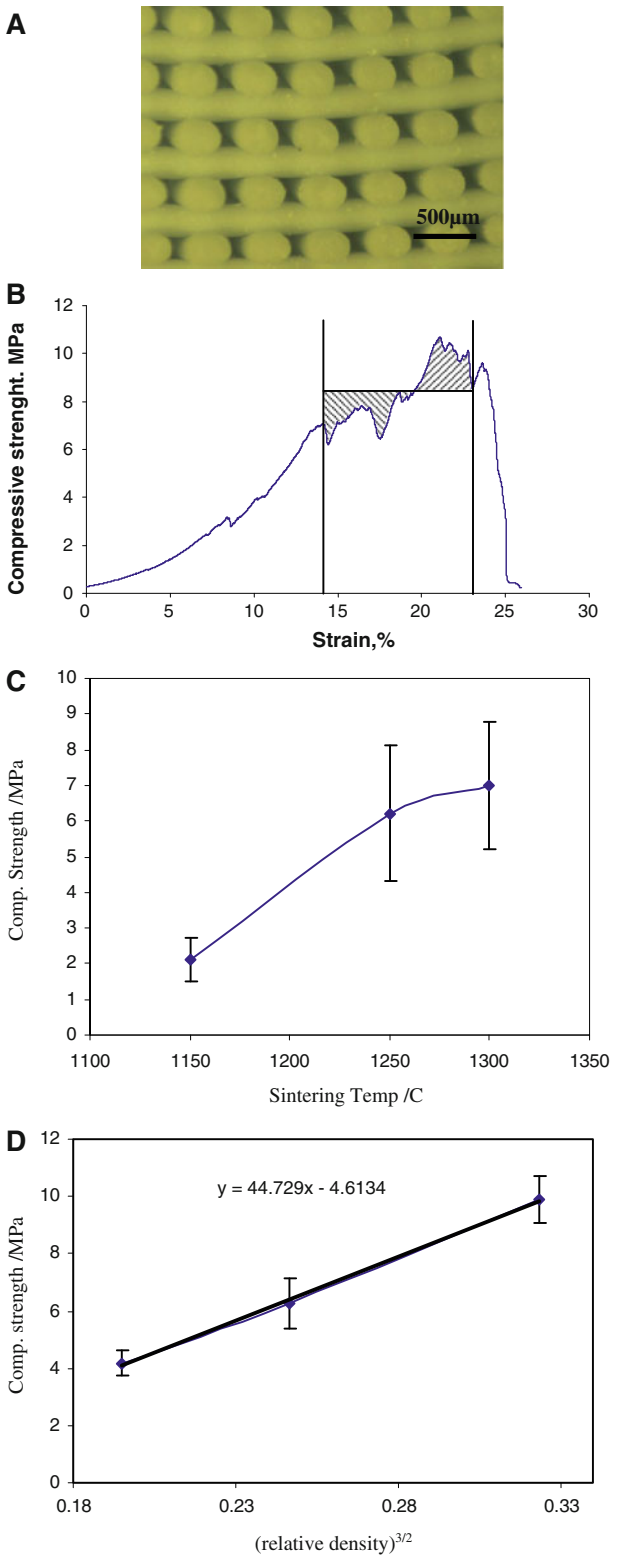

Fig. 4 Compression testing: **a** section showing misalignment resulting from drying deformation, **b** a typical compression testing curve (1250°C, HA with 200 μm gap), **c** the effect of sintering temperature on compressive strength and (d) an Ashby plot for compressive strength versus (relative density)$^{3/2}$

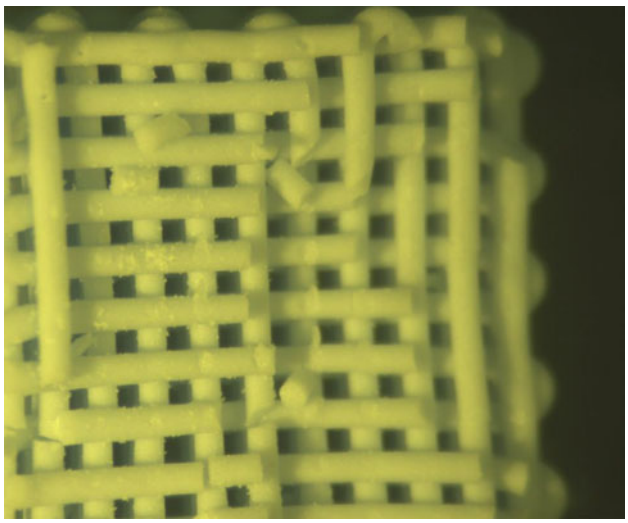

Fig. 5 Typical fracture debris from compression testing of lattices

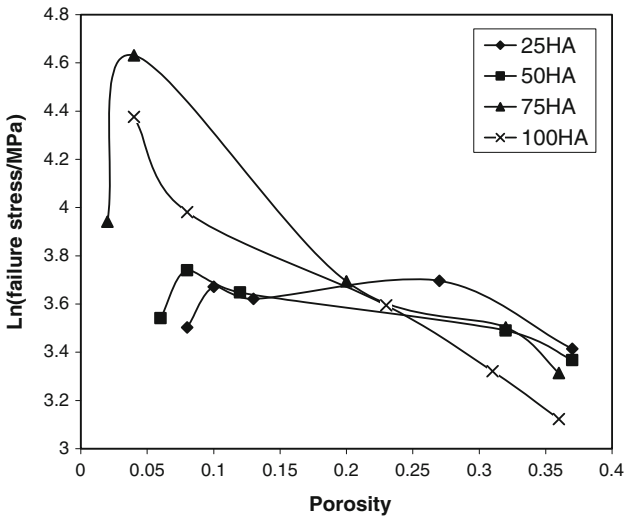

Fig. 6 Natural logarithm of flexural strength (in MPa) plotted as a function of porosity corresponding to Eq. 2

maximum flexural strength of 120 MPa when sintered at 1250°C, the higher strength being partly due to simpler processing than that used here [19]. In our work, the preparation of pastes for extrusion freeforming provides more opportunity for collection of debris from the laboratory environment which can become entrained in the paste and leave pores during heat treatment. Flexural strength measurements on HA–TCP biomaterials by Toriyama et al. [20] also produced values in the region of 100 MPa.

At 1300°C the situation is complicated by phase changes resulting from decomposition to α-TCP [24] and the strengths of all but the 100HA samples fell. Since traces of α-TCP were also found in this sample [24] the fall in

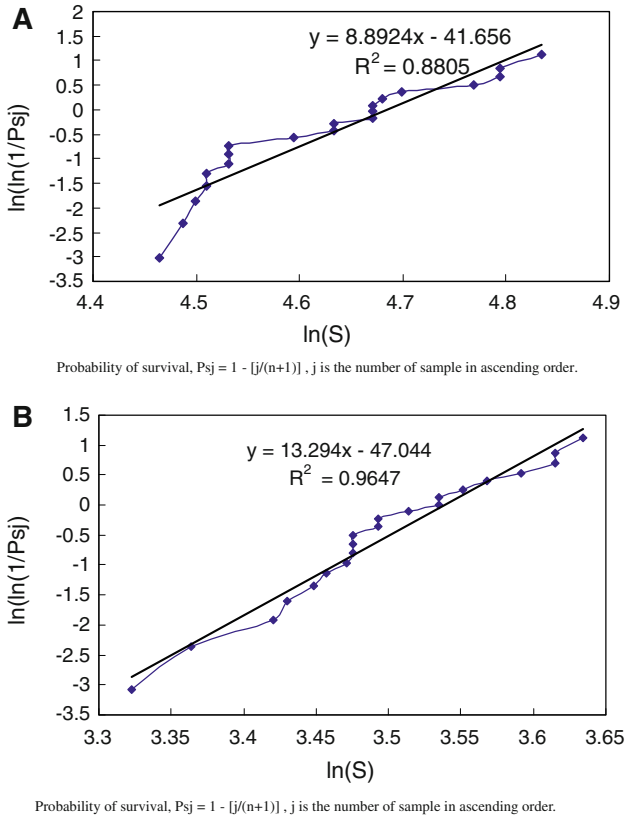

Fig. 7 Weibull plots for filaments of 75HA sintered at **a** 1250°C Weibull modulus, $M = 8.9$ ($n = 20$) and **b** 1150°C Weibull modulus, $M = 13.3$, ($n = 21$)

strength at 1300°C may not entirely be attributable to phase changes; grain growth may also contribute. The reverse but partial transformation α to β occurs during cooling and is accompanied by a specific volume change of about 7% due to the different bulk densities of the polymorphs, inducing residual stresses in densified material.

For monolithic ceramics, a widely used empirical relationship between strength and porosity is:

$$\sigma_f = A \exp(-Bp) \tag{2}$$

in which A is the strength of the fully dense ceramic, p is the fractional porosity and B is an empirical coefficient which has been found to be in the region of 4.5 for previous work on HA [25]. The logarithmic plot suggested by Eq. 2 is quite a good way to present the combined effects of composition and sintering temperature and is shown in Fig. 6. The inability of the 25HA and 50 HA samples to develop strength as sintering progresses is evident and the collapse of strength for 1300°C sintering temperature is clearly seen. When the data point for 75HA at 1300°C is omitted, linear regression for the 75HA and 100HA compositions gives $B = 4.0$ and 3.6, respectively, slightly lower than the value of 4.5 found by Liu for slip cast material [25]. The curves also give a predicted flexural strength at full density (A in Eq. 2) of 109 MPa and 82 MPa, respectively.

If the value of K_{Ic} is taken as 0.9 MPa $m^{1/2}$ after Toriyama et al. [20] who give 0.93 MPa $m^{1/2}$ for a 80–20 HA–TCP ceramic while Liu et al. [19] give 1.2 MPa $m^{1/2}$ for HA both sintered at 1250°C, the critical defect size could be estimated from the engineering form of Griffith's equation for a semicircular flaw and putting the compliance function $Y = 2$ for defects small compared to diameter [26]:

$$c = \left(\frac{\pi K_{Ic}}{4\sigma_f}\right)^2 \tag{3}$$

This gives c in the region of 50 μm. Clearly this is not a valid assessment for two reasons; c/r turns out to be 0.18 so the compliance function $Y \neq 2$ [27]. Second, the cross sections of some filaments have entrapped air bubbles resulting from the extrusion process which are located close to the neutral axis. Although these do not necessarily act as critical defects because of their position they do increase the local compliance and hence change the local stress in the outer fibre of the beam.

Strictly, a valid Weibull modulus plot should have at least 30 points and those shown in Fig. 7a, b for 75HA samples sintered at 1150°C and 1250°C indicate that respectable Weibull moduli are likely to be returned for the flexural strength of these sintered filaments. It is tempting to over-interpret Weibull plots and to see in them different families of defect types each providing a different slope within the overall best fit line. Certainly in these samples different families are expected; entrained air bubbles, entrained debris (from processing in the open laboratory) and local large grains. At a more advanced processing stage, the pastes would be prepared in a glove box using HEPA filtered air and procedures would be in place for de-airing before extrusion.

There remains one anomaly to explain; the high strength shown by 75% HA–25% TCP samples (Table 2). Zyman et al. [28] noted that the literature data for the mechanical properties of hydroxyapatite based ceramics vary widely showing tensile strengths from 20 MPa up to about 200 MPa. The results published by Raynaud et al. [29] on the flexural strength of hot pressed HA/TCP ceramics help to interpret the compositional effect seen in Fig. 6 for the high strength of the 75HA filaments. Their strength reached a maximum of 150 MPa for ceramics containing about 10 wt% of β-TCP but decreased to a minimum of about 75 MPa for pure HA. This could not be related to a variation of the residual porosity or grain size, since material containing up to 30 wt% β-TCP had similar densification

Table 2 Three-point loading flexural strengths, ($n = 6$)

Sintering temperature (°C)	Flexural strength/MPa			
	100HA	75HA	50HA	25HA
1300	79.5 ± 6.5	51.5 ± 7.8	34.5 ± 2.6	33.2 ± 2.8
1250	53.6 ± 4.6	102.7 ± 11.7	42.1 ± 2.9	39.3 ± 2.2
1200	36.4 ± 2.6	40.2 ± 3.3	38.4 ± 2.2	37.4 ± 2.6
1150	27.7 ± 1	33.2 ± 2.6	32.8 ± 1.6	40.3 ± 2
1100	22.7 ± 1.3	27.5 ± 1.6	29 ± 0.3	30.4 ± 3.1

ratios and grain size distributions. Therefore, a small amount of β-TCP (about 10 wt%) doubled the tensile strength of HAP based ceramics.

The variation of mechanical characteristics of their biphasic calcium phosphates (BCP) has been explained in terms of a ceramic–ceramic composite effect [30]. The β-TCP phase is assimilated to a reinforcing second phase dispersed in the HAP matrix. This allows the development of strengthening and/or toughening mechanisms that are effective up to a threshold above which the mechanical properties drop. The threshold depends on the physical properties of the two phases such as thermal expansion coefficient and Young modulus, the morphology and the distribution of the second phase and interfacial strength. In their BCPs this threshold appears to be reached at about 10 wt% β-TCP. Their phase distribution was much finer than the composites produced in our work where samples were made by mixing of powders but the suggestion that a minor proportion of β-TCP enhances mechanical strength is sustained.

4 Conclusions

A wide range of compositions in the hydroxyapatite–β-tricalcium phosphate binary were prepared in the form of extruded filaments and lattice structures sintered from 1100 to 1300°C in steps of 50°C. Compressive strength increased with filament strength and reduced structural porosity. It obeyed the Ashby equation for foams but with a constant $C \sim 0.8$ rather than $C = 2$–3 for ceramic foams, difference attributable to the quite different structure. The flexural strength of the 75 wt% HA–25 wt% TCP filaments was highest, an effect that has been found in biphasic calcium phosphates. The strengths recorded were slightly lower than other reported values for similar material because the laboratory preparation of filaments provided more opportunity for entrained debris and because some filaments contained axially located air bubbles from the extrusion process. Nevertheless, Weibull moduli of up to 13 were recorded from samples of 21 tests.

Acknowledgements The authors are grateful to the Engineering and Physical Sciences Research Council for funding this work under Grant Nos. GR/S57068 and EP/E046193.

References

1. Miyazaki M, Tsumura H, Wang JC, Alanay A. An update on bone substitutes for spinal fusion. Eur Spine J. 2009;18:783–99.
2. Bauer TW. An overview of the histology of skeletal substitute materials. Arch Pathol Lab Med. 2007;131:217–24.
3. Yoshikawa H, Tamai N, Murase T, Myoui A. Interconnected porous hydroxyapatite ceramics for bone tissue engineering. J R Soc Interface. 2009;6:S341–8.
4. Sepulveda P, Binner JGP, Rogero SO, Higa OZ, Bressiani JC. Production of porous hydroxyapatite by the gel-casting of foams and cytotoxic evaluation. J Biomed Mater Res. 2000;50:27–34.
5. Ebaretonbofa E, Evans JRG. High porosity foam scaffolds for bone substitute. J Porous Mater. 2002;9:257–63.
6. Tay BY, Evans JRG, Edirisinghe MJ. Solid freeform fabrication of ceramics. Int Mater Rev. 2003;48:341–70.
7. Yang S, Leong KF, Du Z, Chua CK. The design of scaffolds for use in tissue engineering. Part II: rapid prototyping techniques. Tissue Eng. 2002;8:1–12.
8. Mott M, Evans JRG. Zirconia/alumina functionally graded material made by inkjet printing. Mater Sci Eng A. 1999;271:344–52.
9. Yang S, Mohebi MM, Evans JRG. A novel solid freeforming methodusing simultaneous part and mould construction. Rapid Prototyp J. 2008;14:35–43.
10. Chu TMG, Halloran JW, Hollister SJ, Feinberg SE. Hydroxyapatite implants with designed internal architecture. J Mater Sci. 2001;12:471–8.
11. Peltola SM, Melchels FPW, Grijpma DW, Kellomki M. A review of rapid prototyping techniques for tissue engineering purposes. Ann Med. 2008;40:268–80.
12. Leukers B, Gülkan H, Irsen S, Milz S, Tille C, Schieker M, et al. Hydroxyapatite scaffolds for bone tissue engineering made by 3D printing. J Mater Sci. 2005;16:1121–4.
13. Zein I, Hutmacher DW, Tan KC, Teoh SH. Fused deposition modeling of novel scaffold architectures for tissue engineering applications. Biomaterials. 2002;23:1169–85.
14. Rangarajan S, Qi G, Venkataraman N, Safari A, Danforth SC. Powder processing, rheology, and mechanical properties of feedstock for fused deposition of Si_3N_4 ceramics. J Am Ceram Soc. 2000;83:1663–9.
15. Greul M, Lenk R. Near-net-shape ceramic and composite parts by multiphase jet solidification (MJS). Ind Ceram. 2000;20:115–7.

16. Smay JE, Gratson GM, Shepherd RF, Cesarano J, Lewis JA. Directed colloidal assembly of 3D periodic structures. Adv Mater. 2002;14:1279–83.
17. Fujita R, Yokoyama A, Kawasaki T, Kohgo T. Bone augmentation osteogenesis using hydroxyapatite and beta-tricalcium phosphate blocks. J Oral Maxillofac Surg. 2003;61:1045–53.
18. Peter B, Pioletti DP, Laib S, Bujoli B, Pilet P, Janvier P, et al. Calcuim phosphate drug delivery system: influence of local zoledronate release on bone implant osteointegration. Bone. 2005;36:52–60.
19. Liu HS, Chin TS, Lai LS, Chiu SY, Chung KH, Chang CS, et al. Hydroxyapatite synthesized by a simplified hydrothermal method. Ceram Int. 1997;23:19–25.
20. Toriyama M, Ravaglioli A, Krajewski A, Celotti G, Piancastelli A. Synthesis of hydroxyapatite-based powders by mechanico-chemical method and their sintering. J Eur Ceram Soc. 1996; 16:429–36.
21. Yang HY, Chi XP, Yang S, Evans JRG. Rapid prototyping of ceramic lattices for hard tissue scaffolds. Mater Des. 2008;29: 1802–9.
22. Gibson LJ, Ashby M. Cellular solids: structure and properties. Cambridge, UK: Cambridge University Press; 1999. p. 175–231.
23. Rahaman MN. Ceramic processing and sintering. New York: Marcel Dekker; 2003. p. 486.
24. Yang HY, Yang SF, Chi XP, Evans JRG, Thompson I, Cook RJ, et al. Sintering behaviour of calcium phosphate filaments for use as hard tissue scaffolds. J Eur Ceram Soc. 2008;28:159–67.
25. Liu D-M. Preparation and characterization of porous hydroxyapatite bioceramic via a slip casting route. Ceram Int. 1998;24: 441–6.
26. Davidge RW. Mechanical behaviour of ceramics. Cambridge, UK: Cambridge University Press; 1980. p. 49.
27. Brown WF, Srawley JE. Plane strain crack toughness testing of high strength metallic materials. PA, USA: ASTM Spec. Tech. publ. No.410, ASTM; 1966. p 13.
28. Zyman ZZ, Ivanov IG, Glushko VI. Possibilities for strengthening hydroxapatite ceramics. J Biomed Mater Res. 1999;46:73–9.
29. Raynaud S, Champion E, Lafon JP, Bernache-Assollant D. Calcium phosphate apatites with variable Ca/P atomic ratio III. Mechanical properties and degradation in solution of hot pressed ceramics. Biomaterials. 2002;23:1081–9.
30. Rice RW. Mechanisms of toughening in ceramic matrix composites. Ceram Eng Sci Proc. 1981;2:661–701.